Robotics and Autonomous Systems 96 (2017) 93–101

Contents lists available at ScienceDirect

Robotics and Autonomous Systems

journal homepage: www.elsevier.com/locate/robot

Augmented reality for enhancing tele-robotic system with force feedback

Zhou Zhao, Panfeng Huang *, Zhenyu Lu, Zhengxiong Liu

National Key Laboratory of Aerospace Flight Dynamics, Northwestern Polytechnical University, Xi'an, Shaanxi, 710072, PR China
Research Center for Intelligent Robotics, School of Astronautics, Northwestern Polytechnical University, Xi'an, Shaanxi, 710072, PR China

HIGHLIGHTS

- We presented a method to correctly reconstruct the virtual model of the remote object.
- Our method applies haptic augmented reality technology to the operator site rather than the remote robot site.
- Our method can bring the real-time force feedback to the operator without the effects of the time delay.
- The average relative error between the contact force of the real and the virtual environment is 1.85 ± 0.85%.

ARTICLE INFO

Article history:
Received 30 September 2016
Received in revised form 8 May 2017
Accepted 30 May 2017
Available online 15 June 2017

Keywords:
Augmented reality
Teleoperation
Robot
Force feedback
Haptic

ABSTRACT

In the teleoperation, the force feedback is indispensable, which can enhance the sense of presence of the operator and help the operator accomplish tasks comfortably. The time delay is one of the main challenges that influence the stability of the teleoperation systems, which leads to the discontinuous operation. Thus building a local virtual model in the master side is an effective way to solve this problem. In this paper, a new method is presented to reconstruct the virtual model of the remote object. The virtual model can estimate the real-time force feedback to the operator and eliminate the effects of the time delay. Then the tele-robotic system based on augmented reality technology is set up in our laboratory. In the tele-robotic system, the dynamic parameters including damping and stiffness of the virtual model are constantly updated by utilizing the positions and forces information from sensors of the remote robot site. Finally, the effectiveness of the proposed method and the correctness of the visual model parameters are verified by two experiments.

1. Introduction

Teleoperation has been applied in many research fields such as space robot, high-precision assembly and surgery and so on. It can help the operator accomplish tasks in the dangerous environment and simultaneously bring good sense of presence to the operator, but the existing time delay often generates adverse impact on stability, tracking performance and sense of presence in the teleoperation system.

In order to deal with the problem of time delay in the teleoperation system, numerous methods have been tested by worldwide researchers. The most common methods are predictive aid [1,2], simulation [3], and planning display [4,5]. For example, Dai [6] proposed an original method that compensated the backward wave variable, and the experimental results indicated that the proposed method could keep the system stable. Lu [7] presented a new approach that applied dissymmetric dual-user shared control, which not only changed the training pattern but also improved the flexibility of the teleoperation process. In addition, Sun [8,9] presented a new control algorithm based on modified wave-variable controllers in nonlinear single-master–multiple-slave teleoperation system and even extended his method to apply in the dual-master–dual-slave multilateral teleoperation system, and the experimental results could clearly explain that the proposed method could improve the transparency and stability of the teleoperation system when the system suffered large time delays. Li [10–12] applied adaptive fuzzy control method and adaptive neural network control method to solve the time-vary delays. Similarly, to solve the time delay, some researchers have applied the augmented reality (AR) and virtual reality (VR) technology in the teleoperation system [13–15].

AR technology is mainly derived from VR, and it develops environment where the virtual 3D objects are integrated into a real

* Corresponding author. Fax: +86 29-88460366 x 803
E-mail addresses: zhaozhou@mail.nwpu.edu.cn (Z. Zhao), pfhuang@nwpu.edu.cn (P. Huang), luzhenyu@mail.nwpu.edu.cn (Z. Lu), liuzhengxiong@nwpu.edu.cn (Z. Liu).

http://dx.doi.org/10.1016/j.robot.2017.05.017
0921-8890/

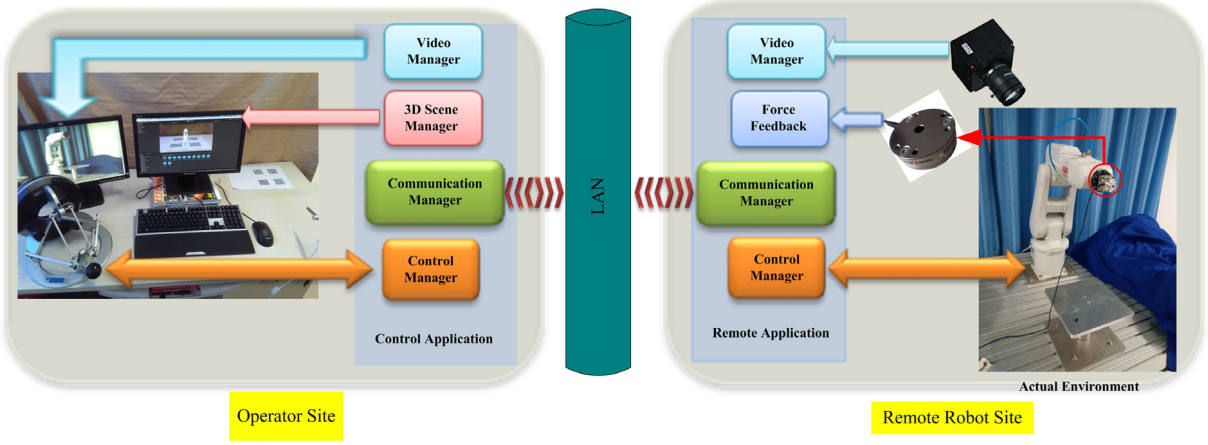

Fig. 1. Tele-robotic system based on AR.

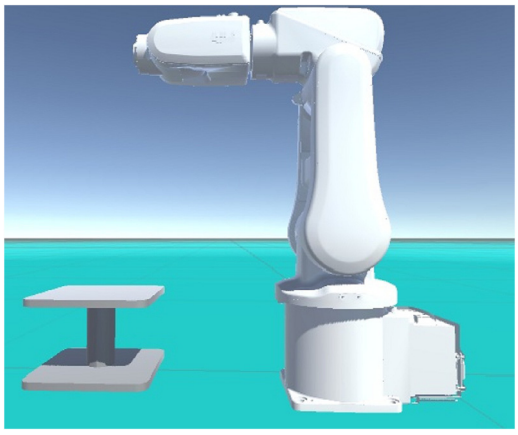

Fig. 2. VR scene.

scene. AR technology has three significant contributions: (1) the real scene and virtual 3D objects are combined together, (2) the virtual 3D objects can be occurred in the real scene by registration and (3) the virtual 3D objects can be controlled in real-time [16]. In the tele-robotic system, utilizing VR and AR technology can improve the security and the efficiency [17]. They can also decrease the influence of time delay by displaying the remote scene in real time at the operator site [18]. Salvatore [19] designed an AR visualization interface, and simultaneously extended his method to further improve the sense of presence of operators by utilizing stereoscopic viewing and 3-D graphics. In order to acquire better interaction among users, Kim [20] designed a convenient and effective teleconference system, and this approach could enhance users' interests and improve the degree of immersion. The advantage of VR and AR technology lies in security, good sense of presence, and convenience [21]. They can provide operators with real-time scene, good sense of presence and the exact virtual model.

Haptic research of the remote object plays an important part of the teleoperation system, and the haptic feedback has been applied to AR systems, simultaneously. Variously previous work is immersed in two categories: visual AR and haptic AR. The virtual AR can be simply explained that virtual objects are incorporated into AR scene without haptic information. Therefore, only the virtual sense is offered. A great deal of previous related work belongs to virtual AR [22–24].

But this paper centers on the haptic rather than the virtual AR. The previous related work about haptic research tries to obtain the virtual haptic sense from the real information that can be acquired by position and force sensors. In order to better accomplish a specific task, using various sensors captures small or noisy signals from a real scene, and the signals can be converted or magnified to the operator site [25,26]. Other research much more concentrates on the combination of virtual haptic sense and real scenes. In these researches, numerous properties are discovered [27–29]. Bayart [30] felt the remote force in the teleoperation system and brought the additional virtual force to an operator. The recent research in this field tries to apply haptic AR technology to medical domain [31], and presents an approach to decompose the contact force [32]. In this paper, the proposed method is significantly different from above methods in several aspects. First, our method applies haptic AR to the teleoperation system, which is different from Bayart's work [30]. Our method correctly reconstructs the virtual model of the remote object by a method that the dynamic parameters including damp and stiffness of the remote object are identified, which not only overcomes the effects of time delay in the teleoperation system, but also brings the real-time force feedback to the operator. Second, the haptic AR technology is applied to the operator site rather than the remote robot site, which can enhance sense of presence of operators and better help operators accomplish tasks.

Therefore, our work focus on the reconstruction of virtual model of the remote real object by utilizing haptic AR technology. The effects of the time delay can be overcame by obtaining the real-time force and visual information feedback from the virtual model. Meanwhile, once the dynamic parameters including the damp and stiffness of remote real objects are identified, the virtual object and the remote real object will be much more similar. The experimental results prove that the virtual force from AR scene and parameters of the visual model are almost correct.

Our paper begins with introducing the tele-robotic system based on AR in Section 2. The remote environment modeling is introduced in Section 3. Section 4 shows the experiment results and discussions. Summarizing remarks and discussions are offered in Section 5.

2. Tele-robotic systems based on AR

Fig. 1 shows the structure of tele-robotic system based on AR technology. It consists of two sites: operator and remote robot, which are connected through a local area network (LAN).

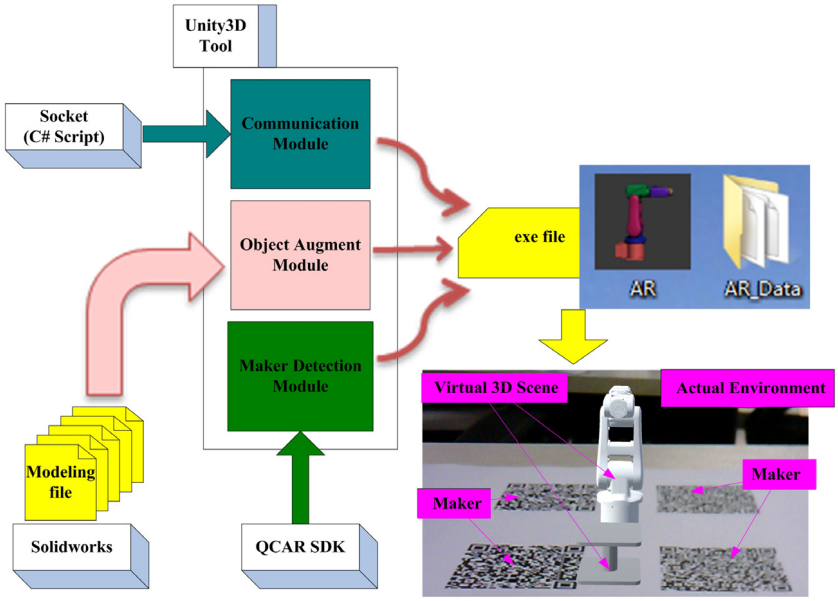

Fig. 3. Overall system structure of the AR scenes.

Table 1
The parameters of the omega haptic device.

Parameter	Numerical value	
workspace	translation	⌀160 mm*L120 mm
force	continuous	12.0 N
resolution	linear	<0.009 mm
stiffness	closed loop	14.5 N/mm
dimensions	height	270 mm
	width	300 mm
	depth	350 mm

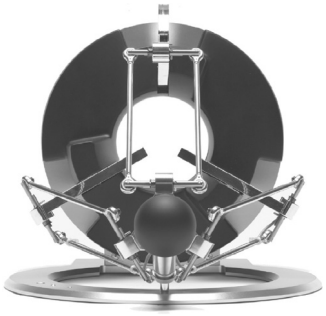

Fig. 4. Omega Haptic Device.

2.1. Operator site

At the operator site, we use Solidworks, 3D modeling software, as the virtual scenarios modeling tool, and Unity3D as the model driver. The virtual model of IRB120 robot that is a size ratio of 1:1 with the real robot is constructed by Solidworks, and operating characteristics of the virtual model are consistent with the real robot. Meanwhile, the VR scene is created by Unity3D (Fig. 2).

We apply QualComm'S Augmented Reality (QCAR) development toolkit to achieve AR scenes, and the QCAR library can be applied in the Unity3D. Fig. 3 shows the overall system structure of AR scenes. It has a QCAR SDK's maker detection module to detect image maker. Also, it has a communication module to connect the remote robot and the operator site. And the augmented module of objects can enhance 3D objects in the screen. All contents from Unity3D edit tool can be set up in forms of executable files, and the executable files can be installed in the windows XP or windows 7.

The Omega (Fig. 4) is a haptic device at the operator site, and operators can control remote robots by it. Table 1 shows the parameters of the Omega Haptic Device. The material of the Omega Haptic Device is light-weight aluminum bars, which is beneficial for the reduction of the inertia. And the stiffness and robustness of the structure are obviously improved due to its parallel mechanics, which can be better applied to the desktop. The Omega has a large workspace (⌀160 mm*L120 mm), a continuous force of 12.0 N, and a closed loop stiffness of 14.5 N/mm. And its performance is more than all other haptic devices. This paper can acquire a high-accuracy result by the Omega.

2.2. Remote robot site

The remote robot site is composed by the IRB120 (Industrial Robot 120) with the IRC5 (Industrial Robot Controller 5), the image capture subsystem, the force sensor, and surrounding environment. The operation of the robot will be done according to planned tasks. The IRB120 is one 6-axis industrial robot of the ABB corporation. The IRC5 is the robotic industry's benchmark in robot controller technology. All ABB robot systems are programmed with RAPID, and the RAPID is a ABB's flexible and high-level programming language. We can keep up a correspondence with a Socket program of the C# language on another computer by applying a Socket program of the RAPID language, and the communication protocol uses the TCP/IP network protocol. The goal of the Socket program of the RAPID language is to enable a RAPID programmer to transmit application data between the computer and the IRC5. By utilizing different Socket programs, a Socket program of the RAPID language on the IRC5 can keep up a correspondence with a Socket program of C/C++ or C# language on another computer.

Table 2
Measurement uncertainty (95% confidence level percent of full-scale load).

F_X	F_Y	F_Z	T_X	T_Y	T_Z
1.50%	1.50%	0.75%	1.75%	1.50%	1.50%

RAPID program for communication on the IRC5 controller

```
MODULE MainModule
    VAR socketdev temp_socket;
    VAR socketdev client_socket;
    VAR string received_string;
    VAR bool keep_listening:=TRUE;
    socketcreate temp_socket;
    socketbind temp_socket, "IP Address", Port;
    socketlisten temp_socket;
    socketaccept temp_socket,client_socket;
    WHILE keep_listening DO
        socketreceive client_socket\Str:=received_string;
        socketsend client_socket\Str:=received_string;
        Packets transference between IRC5 controller and computer;
        Task program of the robot;
        Acquire the data of robot;
    ENDWHILE
    socketclose client_socket;
    socketclose temp_socket;
ENDMODULE
```

The image capture subsystem is composed by a MV-3000UC camera of the Microvision corporation. The camera can connect to a PC running under windows XP. Its goal is to capture the movements at the remote robot site. Then the movements are transmitted to the operator site. The image packets transference in the LAN uses the IP/UDP network protocol in the paper. Although the IP/UDP network protocol does not guarantee the delivery of the image data, it has a faster transmission rate in that it does not spend time checking the arrival of the image packets.

We apply the Mini40 force/torque sensor of the ATI company to acquire force data. The force data is the reaction force between the remote robot and its surrounding objects. And the force data can make us accurately reconstruct the remote objects. The measurement uncertainty for each axis is as follow.

3. Remote environment modeling

In this paper, we use a model replica of the remote objects. This provides better visualization and control without overloading the network. The 3D model of the remote objects is built during the initial system setup process, and once created, the operator can navigate inside this environment as per his viewing requirements.

Fig. 5 shows the block diagram of remote environment modeling. When the operator operates the master arm (Omega Haptic Device), the change of positions of the master arm is transmitted to the slave arm (IRB120) and the AR scene at the operator site through a local area network, respectively. The virtual arm (virtual IRB120) in the AR scene follows the change immediately, which brings the change of visual remote scene to the operator without the effects of the time delay. After a certain time delay, the same change is accomplished by the slave arm, and the information of precise positions and forces can be obtained by position and force sensors of the remote robot site, simultaneously. Then the dynamic parameters including damping and stiffness of the remote objects are identified by using the information of precise positions and forces, and simultaneously they are applied to update the dynamic parameters of the corresponding objects in the AR scene. The object of the remote robot site is reconstructed at the operator site, which can improve the operating accuracy of operators.

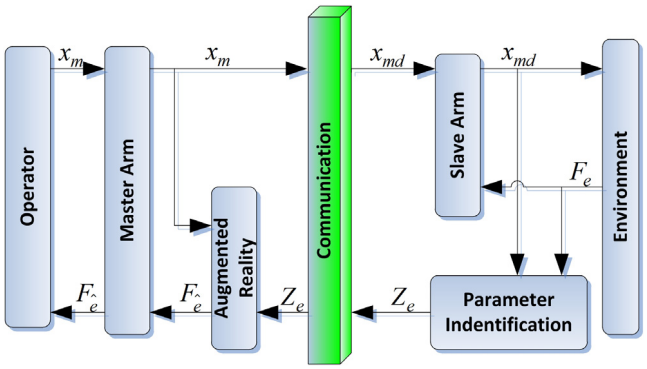

Fig. 5. Block diagram of remote environment modeling.

3.1. Dynamic model of the environment

The dynamic model can clearly explain the relation between the slave arm (IRB120) and the surrounding objects. Therefore, building the dynamic model is indispensable.

The model of collision is divided into two parts: (a) the elastic force between two bodies due to mutual penetration depth. (b) the damping force deriving from the relative velocity of two bodies. The model can be denoted by the following equation:

$$F_e = k(x_e)^n + \lambda(x_e)^n \dot{x}_e \tag{1}$$

where k and λ denote the local contact stiffness coefficient and damping coefficient at the position of collision respectively. x_e denotes the penetration depth between two bodies along the z-axis (Fig. 8a). $\dot{x}_e$ denotes the relative velocity at the contact position. n denotes the exponent of collision and it indicates the nonlinearity extent of the material. n is 1.5 in this paper, and k is obtained by a method from Zhang's work [33], but the method is aimed at curvilinear motion, therefore, k can be obtained by

$$k = \frac{4\tau}{3\pi\,(\sigma_1 + \sigma_2)} \tag{2}$$

where τ denotes a constant, but different motion paths cause the change of the value of τ in the contact process, and the value of τ is 1 in this paper. The material parameters σ_1 and σ_2 can be obtained by

$$\sigma_i = \frac{1 - v_i^2}{\pi E_i},\ i = 1, 2 \tag{3}$$

where E_i denotes the elastic modulus and v_i denotes Poisson's ratio with each contacting bodies. In this paper, the elastic modulus of the experiment object is 2.8×10^9 N/m^2, and the Poisson's ratio is 0.38. The elastic modulus of the robot end-effector is 7×10^{10} N/m^2, and the Poisson's ratio is 0.33.

To calculate damping coefficient λ, numerous algorithms have been presented by world-wide researchers. At present, the expression of damping coefficient λ has several different classical models:
(1) Flores [34]

$$\lambda = \frac{8\,(1 - c_r)}{5c_r}\frac{k}{\dot{x}_e^-}. \tag{4}$$

(2) Gonthier [35]

$$\lambda = \frac{1 - c_r^2}{c_r}\frac{k}{\dot{x}_e^-}. \tag{5}$$

(3) Lankarani–Nikravesh [36]

$$\lambda = \frac{3\left(1 - c_r^2\right)}{4}\frac{k}{\dot{x}_e^-}. \tag{6}$$

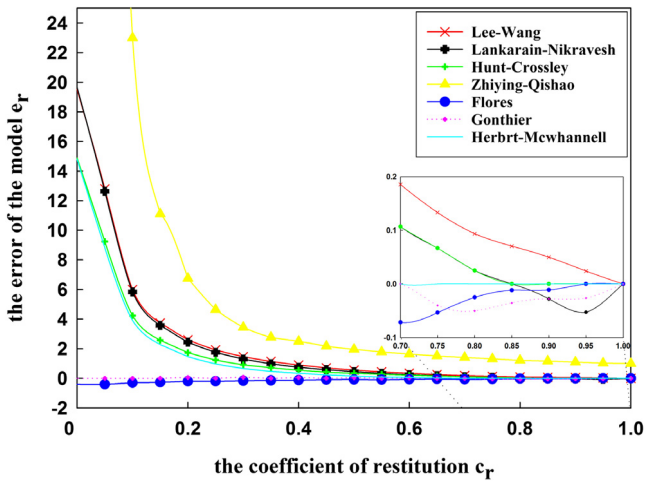

Fig. 6. Accuracy comparison of seven models.

(4) Lee–Wang [37]

$$\lambda = \frac{3\left(1 - c_r\right)}{4} \frac{k}{\dot{x}_e^-}. \tag{7}$$

(5) Hunt–Crossley [38]

$$\lambda = \frac{3\left(1 - c_r\right)}{2} \frac{k}{\dot{x}_e^-}. \tag{8}$$

(6) Zhiying–Qishao [39]

$$\lambda = \frac{3\left(1 - c_r^2\right) e^{2(1-c_r)}}{4} \frac{k}{\dot{x}_e^-}. \tag{9}$$

(7) Herbert–McWhannell [40]

$$\lambda = \frac{6\left(1 - c_r\right)}{\left[(2c_r - 1)^2 + 3\right]} \frac{k}{\dot{x}_e^-}. \tag{10}$$

The damping coefficient denotes the energy loss of collision. c_r denotes the coefficient of restitution and it indicates the recovery capability of the collision object deformation. c_r rests with the collision object material. $\dot{x}_e^-$ denotes a relative velocity at the collision position before the collision.

The coefficient of restitution c_r can be obtained by

$$c_r = \frac{\partial^T \left(\dot{x}_{P\_object}^- - \dot{x}_{P\_end}^-\right)}{\partial^T \left(\dot{x}_{e\_end}^- - \dot{x}_{e\_object}^-\right)} \tag{11}$$

where ∂ denotes the unit vector of the collision direction. $\dot{x}_{P\_object}^-$ and $\dot{x}_{e\_object}^-$ are, respectively, the velocity of the experiment object after the collision and before the collision. $\dot{x}_{P\_end}^-$ and $\dot{x}_{e\_end}^-$ are, respectively, the velocity of the robot end-effector after the collision and before the collision.

In order to accurately express the collision process, we present a criterion to reasonably choose above seven models: the model error can be obtained by

$$e_r = \frac{\dot{x}_M^+ - \dot{x}_P^-}{\dot{x}_P^-} = \frac{c_{r\_M} - c_r}{c_r} \tag{12}$$

where $c_{r\_M} = \dot{x}_M^+ / \dot{x}_e^-, \dot{x}_P^- = -c_r \dot{x}_e^-. \dot{x}_P^-$ denotes the theoretical relative velocity after the collision. $\dot{x}_M^+$ denotes actual relative velocity after the collision, which can be obtained by Eqs. (1) to (10).

Fig. 6 shows the accuracy comparison of seven models. If c_r is a constant value, obtaining e_r will be different by seven models, so for the different value of c_r, we should choose a suitable model in the seven models. Gonthier and Flores models keep a minor error all the time when the value of c_r belongs to a range from 0 to 1. With the increase of the value of c_r, the model error of Lee–Wang, Hunt–Crossley, Lankarani–Nikravesh, Zhiying–Qishao, and Herbert–McWhannell models gradually decrease. However, when the value of c_r belongs to a range from 0.7 to 1, the model error of Herbert–McWhannell is minimum. The value of c_r is 0.8 in this paper, so we choose the Herbert–McWhannell model, λ can be obtained by Eq. (10).

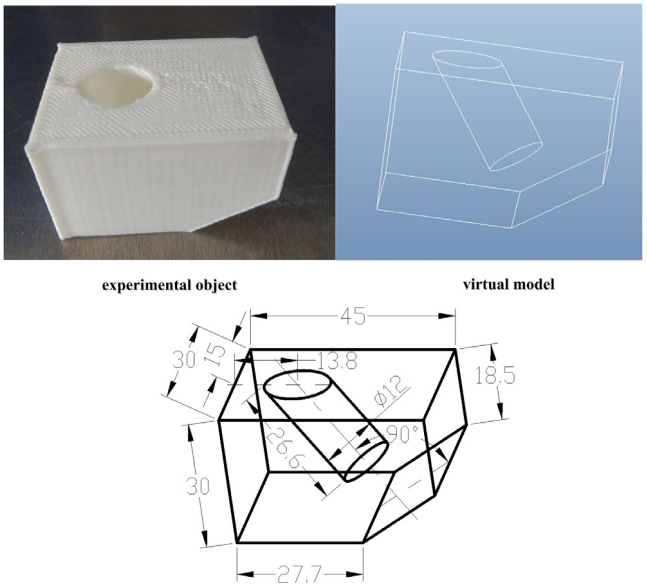

Fig. 7. The architecture of experiment object.

The primary goal in this paper is to bring the real-time force and visual information feedback to the operator without the effects of the time delay by correctly reconstructing the remote physical environment despite they are delayed, which is well built in that the force and visual information immediately feedback enhances the sense of presence of the operator.

4. Experiment results and discussions

In this section, we set up a tele-robotic system with AR experiment. Fig. 7 shows the architecture of experiment object. The experiment object material is polylactide (PLA), and the experiment object is manufactured by 3D printer. The operator controls the remote robot by operating master arm (Omega haptic device). The experiment includes two cases: (a) obtaining the parameters of the remote objects by the contact experiment. (b) verifying the parameters of the remote object by the hole slotting experiment.

4.1. Contact experiment

In order to acquire the parameters including stiffness and damping of the remote experiment object, we conduct a contact experiment. We control the robot end-effector to contact the experiment object with different z-axis velocity (5, 10, 20, 30, 40, 50, and 60 mm/s). And the experiment object deformation is 2 mm along z-axis, so the penetration depth x_e is 2 mm. Fig. 8a shows the contact experiment based on the real word, and Fig. 8b shows the contact experiment based on the AR.

Fig. 9 shows the results of the contact experiment. We can acquire the parameters of the remote experiment object including damp and stiffness from the results of the contact experiment in the real environment through the method of parameter identification. Fig. 9b is the results of the contact experiment in the AR

Table 3
The maximum contact force of the contact experiment of different velocities.

Velocity/mm/s	Real environment/N	AR scene/N	The relative errors between the real environment and the AR scene/%
5	22.41	22.85	1.96
10	21.57	21.73	0.74
20	18.97	18.35	3.27
30	16.87	16.60	1.60
40	19.21	18.68	2.76
50	18.88	19.06	0.95
60	17.49	17.20	1.66

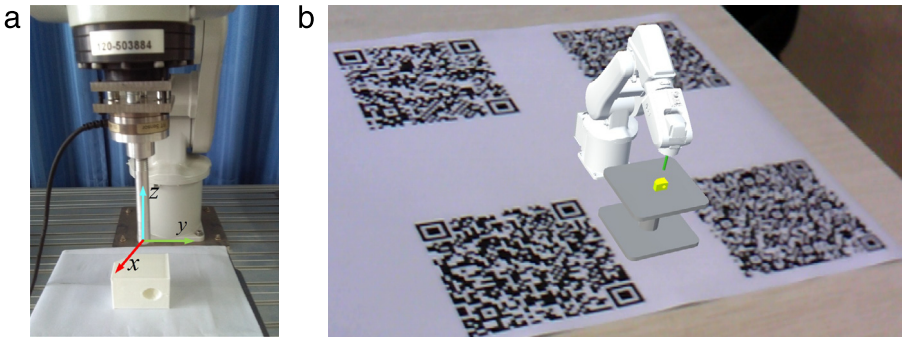

Fig. 8. Contact experiment. (a) The contact experiment based on the real word. (b) the contact experiment based on the AR.

scene corresponding the results of the real environment, which verifies that the AR scene is almost correctly reconstructed. The consuming time of Fig. 9a is different from Fig. 9b for different experiment velocities, because the results of Fig. 9a is obtained by the remote robot, and the motion of the remote robot is restricted to the fixed velocity, but the operator operates master arm (Omega Haptic Device) with uncertain velocities at the operator site, which will lead to the virtual robot reaches the designated position with different velocities. Compared the experiment results of Fig. 9a and Fig. 9b, we can clearly obtain a conclusion that the force feedback of the real world almost is same as the AR scene, but there are still differences between the z-axis contact force of the real environment and the AR scene. This lies in mainly two factors: (1) the sensor error due to the measurement uncertainty for the z-axis (Table 2), (2) the parameter identification error due to the actual friction noises of information detection. Table 3 shows the maximum contact force of the contact experiment of different velocities. The average relative error between the z-axis contact force of the real and the virtual environment is 1.85±0.85%.

4.2. Hole slotting experiment

In order to verify the parameters of the remote object that is obtained through the contact experiment, we continue to design a hole slotting experiment. It imitates a real robot assignment. Meanwhile, the experiment object is a given shape, which aims to achieve a process that the operator is affected by the force feedback from the AR scene, and then the operator adjusts the way of the operation to better adapt to the change of the remote object and accomplish the assignment.

Fig. 10a shows the hole slotting experiment based on the real world. Fig. 10b shows the hole slotting experiment based on the AR. The movement of the robot end-effector is restricted to z-axis during the whole hole slotting experiment, and the hole of the experiment object is oblique, which both aims to make the operator feels the change of the force, and make the adjustment to accomplish the hole slotting experiment. The velocity of the robot end-effector is variable in the operator control process, but it is not greater than 60 mm/s.

Fig. 11 shows the result of the hole slotting experiment. The experimental results verify the validity of parameters obtaining

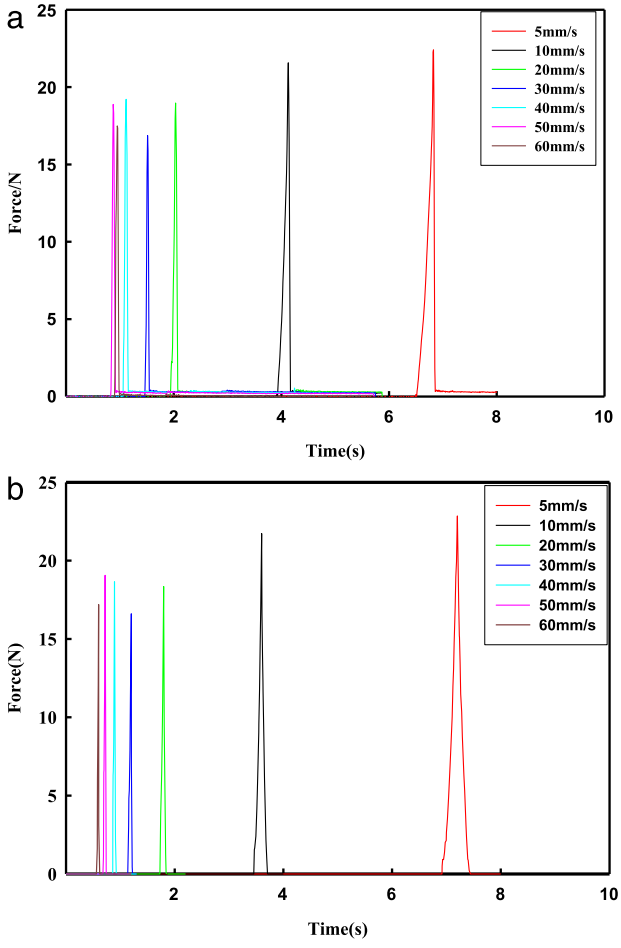

Fig. 9. The results of the contact experiment. (a) The z-axis contact force of the real environment. (b) The z-axis contact force of the AR scene.

from the contact experiment. In the movement process from the first position to the second position, the force of z-axis is 0N,

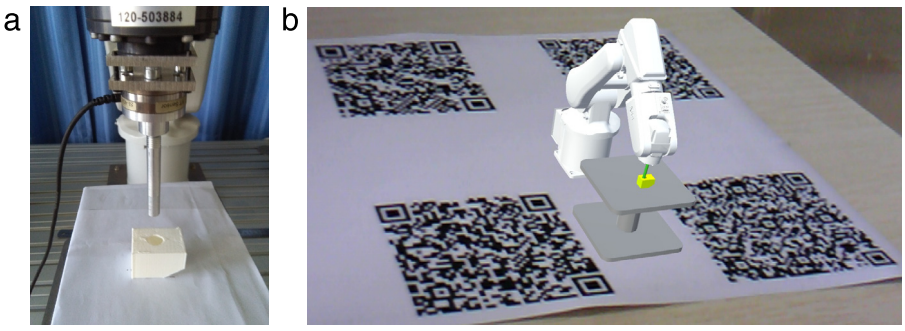

Fig. 10. Hole slotting experiment. (a) The hole slotting experiment based on the real world. (b) The hole slotting experiment based on the AR.

because the contact of two bodies does not happen. From the second position to the third position, the cylinder stick and the experimental object interact on each other. The cylinder stick slides along the slope of the hole, and the experimental object is compelled to slide along the y-axis in that the movement of the robot end-effector is restricted to z-axis. From the third position to the fourth position, the force of z-axis rapidly decreases to 0N, because the experiment object is compelled to revolve round x-axis, which causes the contact force decline. From the fourth position to the fifth position, the cylinder stick moves to the bottom of the hole, and the force of z-axis reaches to the maximum value. By comparing the z-axis contact force of the real environment and the AR scene, we can find that their trajectory curve is similar, and the force also almost is same. The hole slotting experiment verifies that the parameters of the remote object from the contact experiment almost are correct. Meanwhile, it also indicates that the operator can better accomplish the assignment by correctly reconstructing the remote object in that the operator can feel the real-time force feedback without the effects of the time delay in the tele-robotic system. The maximum value of the z-axis contact force in the real environment and the AR scene are 91.23 and 93.27N, respectively. Therefore, the relative error between the maximum value of the z-axis contact force in the real environment and the AR scene is 2.24%.

4.3. Compare experiment

We conduct a pair of experiments to show the advantages of the proposed method from two aspects: the haptic teleoperation method and two state-of-the-art methods. According to the recent article [41], a method that the plastic object retrieves the workpiece geometry from a file and the corresponding action template from the database is proposed, but the virtual model is not changeable during the operation process. The case is hard to be realized in reality, because it needs a prior knowledge of the environment before reconstructing the virtual model. This paper presents a novel adaptive changing model method. Compared to reference [41], we conduct a similar experiment to Ref. [41]. Fig. 12 presents the physical side and the virtual side of the experimental platform. Fig. 12a shows the real solo-arm robot in the real world. Fig. 12b shows the equipment in the virtual environment. In the compare experiment, the rigid material in Fig. 9 is replaced by the plastic soft blue ball. Here, we make a brief introduction about the experimental setup. Firstly, we control the robot end-effector to contact the plastic ball with different velocities (10, 20, 30, 40, and 50 mm/s) along z-axis. Secondly, the proposed method of section 3 is utilized to identify and correct the dynamic parameters of the virtual model. The force information are measured with the same time interval 0.1 s. And Fig. 13 shows the real and the virtual values of the contact force. Form the result of the experiment, we can make a conclusion that the virtual and real force is almost same,

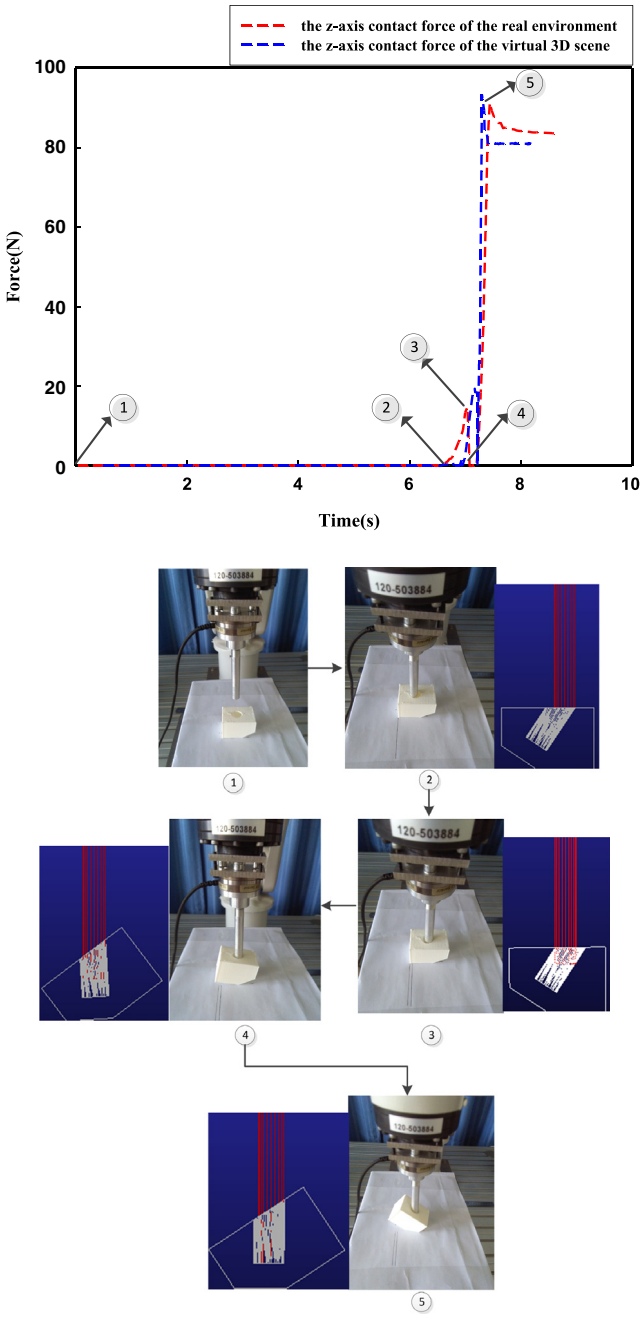

Fig. 11. The results of the hole slotting experiment.

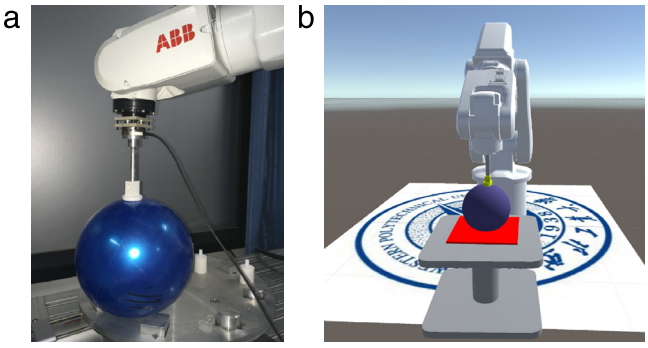

Fig. 12. Compare experiment. (a) The compare experiment based on the real world. (b) The compare experiment based on the virtual reality.

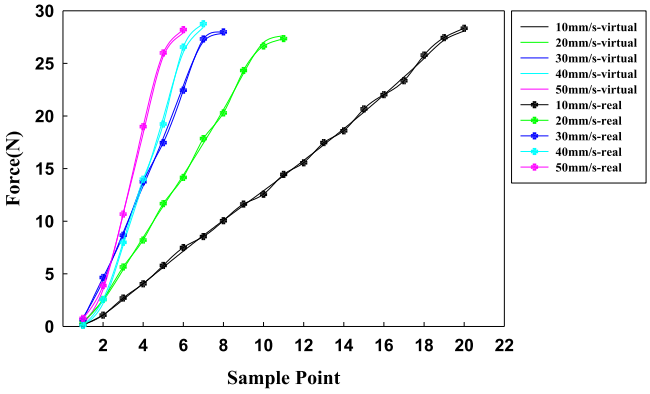

Fig. 13. The result of compare experiment.

Table 4
The relative error of three methods.

Method	The relative error%
Our	2.24
GADM	2.75
HSMM	3.12

and the contact forces have a linear relationship with velocities, so the evaluating fitting degree with different contact velocities is better than the result of the rigid contact. For the comparison, the advantages of our method are obvious. Our method applies the haptic AR technology to the operator site and constantly corrects the dynamic parameters of the virtual model, which makes the virtual model gradually close to the correct model and enhances sense of presence of operators. In addition, our method is suitable for both rigid material and the plastic material without any prior knowledge, which denotes that our method is better suitable for the task environment of robot than Ref. [41].

Furthermore, we compare the proposed method with two state-of-the-art methods. Two methods are GADM (Geometric and Dynamic Models) [42]. GADM can provide the operator with appropriate predictive virtual forces with a certain time delay, and HSMM-CIC can modulate the stiffness smoothly during the reproduction of the dynamic model, which is suitable for modeling the dynamics of in-contact tasks. Table 4 shows the relative error of three methods. Compared to GADM and HSMM-CIC, the relative error of our method is minimum.

5. Conclusion

This paper presents a novel method to reconstruct the virtual model of the remote real object. The effects of the time delay can be overcame by obtaining the real-time force and visual information feedback from the AR scene. Meanwhile, once the dynamic parameters including the damp and stiffness of remote real object are identified, the virtual object and the remote real object will be much more similar. The experimental results prove that the virtual force from AR scene and parameters of visual model are almost correct, and the average relative error between the z-axis contact force of the real and the virtual environment is 1.85±0.85%.

Acknowledgment

This research is sponsored by the National Natural Science Foundation of China (Grant No: 11272256, 61005062, 60805034).

References

[1] C. Smith, P. Jensfelt, A predictor for operator input for time-delayed teleoperation, Mechatronics 20 (7) (2010) 778–786.
[2] Y.J. Pan, C. Canudas-de Wit, O. Sename, A new predictive approach for bilateral teleoperation with applications to drive-by-wire systems, IEEE Trans. Robot. 22 (6) (2006) 1146–1162.
[3] H.J. Li, A.G. Song, Virtual-environment modeling and correction for force-reflecting teleoperation with time delay, IEEE Trans. Ind. Electron. 54 (2) (2007) 1227–1233.
[4] J. Aleksandar, D. Guillaume, P. Yisrael, et al., Comparison of interaction modalities for mobile indoor robot guidance: direct physical interaction, person following, and pointing control, IEEE Trans. Human-Mach. Syst. 45 (6) (2015) 653–663.
[5] G. Adamides, G. Christou, C. Katsanos, et al., Usability guidelines for the design of robot teleoperation: a taxonomy, IEEE Trans. Human-Mach. Syst. 45 (2) (2015) 256–262.
[6] P. Dai, P. F. Huang, Z. Y. Lu, Time Delayed teleoperation with stable tracking and high feedback fidelity using modified wave variable, in: 2015 IEEE International Conference on Robotics and Biomimetics, ROBIO, Zhuhai, 2015, pp. 476–480.
[7] P. F. Huang, Z. Y. Lu, Auxiliary asymmetric dual-user shared control method for teleoperation, in: 2015 12th International Conference on Ubiquitous Robots and Ambient Intelligence, URAI, Goyang, 2015, pp. 267–272.
[8] D. Sun, F. Naghdy, H. Du, Transparent four-channel bilateral control architecture using modified wave variable controllers under time delays, Robotica 34 (4) (2014) 859–875.
[9] D. Sun, F. Naghdy, H. Du, Enhancing flexibility of the dual-master-dual-slave multilateral teleoperation system, in: 2015 IEEE Conference on Control Applications, CCA, Sydney, 2015, pp. 300–305.
[10] Z.J. Li, L. Ding, H.B. Gao, Trilateral teleoperation of adaptive fuzzy force/motion control for nonlinear teleoperators with communication random delays, IEEE Trans. Fuzzy Syst. 21 (4) (2013) 610–624.
[11] Z.J. Li, X.Q. Gao, N. Ding, Adaptive fuzzy control for synchronization of nonlinear teleoperators with stochastic time-varying communication delays, IEEE Trans. Fuzzy Syst. 19 (4) (2011) 745–757.
[12] Z.J. Li, C.Y. Su, Neural-adaptive control of single-master- multiple-slaves teleoperation for coordinated multiple mobile manipulators with time-varying communication delays and input uncertainties, IEEE Trans. Neural Netw. Learn. Syst. 24 (9) (2013) 1400–1433.
[13] A. Bolopion, S. Régnier, A review of haptic feedback teleoperation systems for micromanipulation and microassembly, IEEE Trans. Autom. Sci. Eng. 10 (3) (2013) 496–502.
[14] K. Chintamani, A. Cao, R.D. Ellis, et al., Improved telemanipulator navigation during display-control misalignments using augmented reality cues, IEEE Trans. Syst. Man Cybern. A 40 (1) (2010) 29–39.
[15] Q.Z. Ang, B. Horan, S. Nahavandi, Multipoint haptic mediator interface for robotic teleoperation, IEEE Syst. J. 9 (1) (2015) 86–97.
[16] M. Gianni, F. Ferri, F. Pirri, ARE: Augmented Reality Environment for Mobile Robots, in: Towards Autonomous Robotic Systems, Springer, Berlin, Heidelberg, 2013, pp. 470–483.
[17] M. Hayashibe, N. Suzuki, M. Hashizume, et al., Preoperative planning system for surgical robotics setup with kinematics and haptics, Int. J. Med. Robot. Comput. Assist. Surg. 1 (2) (2005) 76–85.
[18] Y. Xiong, S. Li, M. Xie, Predictive display and interaction of telerobots based on augmented reality, Robotica 24 (4) (2006) 447–453.
[19] L. Salvatore, B. Filippo, M. Giovanni, 3-D Integration of Robot Vision and Laser Data With Semiautomatic Calibration in Augmented Reality Stereoscopic Visual Interface, IEEE Trans. Ind. Inform. 8 (1) (2012) 69–77.
[20] H.H. Kim, J.S. Park, J.W. Jung, et al., Immersive teleconference system based on human-robot-avatar interaction using head-tracking devices, Int. J. Control Autom. Syst. 11 (5) (2013) 1028–1037.

[21] M. Hayashibe, N. Suzuki, M. Hashizume, et al., Preoperative planning system for surgical robotics setup with kinematics and haptics, Int. J. Med. Robot. Comput. Assist. Surg. 1 (2) (2005) 76–85.
[22] M. Harders, G. Bianchi, B. Knorlein, et al., Calibration, registration, and synchronization for high precision augmented reality haptics, IEEE Trans. Vis. Comput. Graphics 15 (1) (2009) 138–149.
[23] S. Jeon, S. Choi, Haptic augmented reality: taxonomy and an example of stiffness modulation, Presence: Teleoper. Virtua Environ. 18 (5) (2009) 387–408.
[24] R. Ott, D. Thalmann, F. Vexo, Haptic feedback in mixed-reality environment, Vis. Comput.: Int. J. Comput. Graphics 23 (9) (2007) 843–849.
[25] H. Kajimoto, N. Kawakami, S. Tachi, et al., Smart touch: electric skin to touch the untouchable, IEEE Comput. Graph. Appl. 24 (1) (2004) 36–43.
[26] T. Nojima, D. Sekiguchi, M. Inami, The SmartTool: A System for Augmented Reality of Haptics, in: Proceedings of the IEEE Virtual Reality Conference, 2002, pp. 67–72.
[27] C.W. Borst, R.A. Volz, Evaluation of a haptic mixed reality system for interactions with a virtual control panel, Presence: Teleoper. Virtual Environ. 14 (6) (2005) 677–696.
[28] K.U. Kyung, J.Y. Lee, Ubi-pen: a haptic interface with texture and vibrotactile display, IEEE Comput. Graph. Appl. 29 (1) (2009) 56–64.
[29] Z.F. Quek, S.B. Schorr, I. Nisky, et al., Augmentation of stiffness perception with a 1-degree-of-freedom skin stretch device, IEEE Trans. Human-Mach. Syst. 44 (6) (2014) 731–742.
[30] B. Bayart, J.Y. Didier, A. Kheddar, Force feedback virtual painting on real objects: a paradigm of augmented reality haptics, Lecture Notes in Computer Science, vol. 5024, pp. 776–785, (2008).
[31] S. Jeon, S. Choi, H. Matthias, Rendering virtual tumors in real tissue mock-ups using haptic augmented reality, IEEE Trans. Haptics 5 (1) (2012) 77–84.
[32] H. Kim, S. Choi, W. K. Chung, Contact force decomposition using tactile information for haptic augmented reality, in: 2014 IEEE/RSJ International Conference on Intelligent Robots and Systems, IROS, Chicago, 2014, pp. 1242–1247.
[33] L. Zhang, Q. Jia, G. Chen, et al. Impact analysis of space manipulator collision with soft environment, in: 2014 IEEE 9th Conference on Industrial Electronics and Applications, ICIEA, Hangzhou, 2014, pp. 1965–1970.
[34] P. Flores, M. Machado, M.T. Silva, J.M. Martins, On the continuous contact force models for soft materials in multibody dynamics, Multibody Syst. Dyn. 25 (3) (2011) 357–375.
[35] Y. Gonthier, J. McPhee, C. Lange, J.C. Piedboeuf, A regularized contact model with asymmetric damping and dwell-time dependent friction, Multibody Syst. Dyn. 11 (3) (2004) 209–233.
[36] H.M. Lankarani, P.E. Nikravesh, A contact force model with hysteresis damping for impact analysis of multibody systems, J. Mech. Des. 112 (3) (1990) 369–376.
[37] T.W. Lee, A.C. Wang, On the dynamics of intermittent-motion mechanisms, part 1: dynamic model and response, J. Mech. Transm. Autom. Des. 105 (3) (1983) 534–540.
[38] K.H. Hunt, F.R.E. Crossley, Coefficient of restitution interpreted as damping in vibroimpact, J. Appl. Mech. 42 (2) (1975) 440–445.
[39] Z.Y. Qin, Q.S. Lu, Analysis of impact process based on restitution coefficien, J. Dyn. Control (2006) 294–298.
[40] R.G. Herbert, D.C. McWhannell, Shape and frequency composition of pulses from an impact pair, J. Eng. Ind. 99 (3) (1977) 513–518.
[41] Y. Wu, W. L. Chan, Y. Li, Improving human-robot interactivity for tele-operated industrial and service robot applications, in: 2015 IEEE 7th International Conference on Cybernetics and Intelligent Systems (CIS) and IEEE Conference on Robotics, Automation and Mechatronics (RAM), Siem Reap, 2015, pp. 153–158.
[42] R. Mattia, P. Joni, M. Alberto, et al., Learning in-contact control strategies from demonstration, in: 2016 IEEE/RSJ International Conference on Intelligent Robots and Systems, IROS, Daejeon, 2016, pp. 688–695.

Zhou Zhao received his B.S. degree from the Northwest Agriculture and Forestry University in 2015. He is now a postgraduate student of Astronautics in Northwestern Polytechnical University. His research interests are focused on computer vision, man–machine interaction and teleoperation.

Panfeng Huang Professor, School of Astronautics, Northwestern Polytechnical University and the National Key Laboratory of Aerospace Flight Dynamics. He received B.S. and M.S. degree from Northwestern Polytechnical University in 1998, 2001, respectively, and Ph.D. from the Chinese University of Hong Kong in the area of Automation and Robotics in 2005. He is currently a Professor of School of Astronautics and Vice Director of Research Center for Intelligent Robotics at the Northwestern Polytechnical University. His research interests include tethered space robotics, intelligent control, machine vision, space teleoperation.

Zhenyu Lu received his B.S. and M.S. degree from China University of Mining and Technology and Shenyang Aerospace University in 2010 and 2012 respectively. He is currently a Ph.D. candidate of School of Astronautics, Northwestern Polytechnical University. His research interests include space teleoperation, man–robotics interaction and system identification.

Zhengxiong Liu received the Ph.D. degree from Northwestern Polytechnical University, Xi'an, China, in 2012. He is currently a Lecturer with the School of Astronautics, Northwestern Polytechnical University. His research interests include space teleoperation, multibody dynamics, and man–machine interaction.